

A fourteen peripherally fluorinated dimeric acceptor enables organic solar cells achieve 19.7 % efficiency

Shuhui Ding^{a,1}, Xingqi Bi^{a,1}, XiangJian Cao^a, Jinyi Yang^a, Huazhe Liang^a, Zhaoyang Yao^{a,*}, Guankui Long^b, Yaxiao Guo^c, Chenxi Li^a, Xiangjian Wan^a, Yongsheng Chen^{a,*}

^a State Key Laboratory and Institute of Elemento-Organic Chemistry, The Centre of Nanoscale Science and Technology and Key Laboratory of Functional Polymer Materials, Renewable Energy Conversion and Storage Center (RECAST), Frontiers Science Center for New Organic Matter, College of Chemistry, Nankai University, Tianjin 300071, China

^b School of Materials Science and Engineering, National Institute for Advanced Materials, Renewable Energy Conversion and Storage Center (RECAST), Nankai University, Tianjin 300350, China

^c State Key Laboratory of Separation Membranes and Membrane Processes, School of Chemistry, Tiangong University, Tianjin 300387, China

ARTICLE INFO

Keywords:

Organic solar cell
Oligomeric small-molecule acceptor
14 peripheral fluorination
High fill factor

ABSTRACT

The oligomeric small-molecule acceptors (OSMAs) could combine the advantages of small-molecule acceptors (SMAs) and polymerized acceptors (PSMAs), including the definite molecular structures, high glass transition temperatures and low diffusion rates. However, a reduction in molecular symmetry and planarity usually decreases the intermolecular stacking strength and ordering, thus lowering the power conversion efficiencies (PCEs) of organic solar cells (OSCs). Herein, the maximum fluorination was conducted on the periphery of two-dimensional plane of OSMA, rendering a 14 fluorine-containing dimeric acceptor of CH14F which affords the most fluorine-rich molecular backbone among all the OSMAs currently. The sufficient peripheral fluorination of backbone leads to more compact and orderly molecular packing and consequently improved the fill factor of OSCs. As a result, the PM6:CH14F:CH6 ternary device achieved a first-class PCE of 19.72 %. More importantly, the PM6:CH14F device retained over 80 % of initial PCE after being continuously heated at 65 °C for 1032 h. Our work demonstrates that implementing sufficient peripheral fluorination on OSMAs could conquer the molecular stacking disorder through the significantly enhanced fluorine-induced secondary interactions, thereby providing a new insight into OSCs with excellent efficiency and stability simultaneously.

1. Introduction

Organic solar cells (OSCs), which utilize modifiable organic materials as their photosensitive active layer, offer distinct advantages including translucency, flexibility, lightweight design, and large-scale production [1]. In addition to serve as a power generation device, these features make OSCs particularly promising for applications in areas such as wearable devices that has sparked significant interest from both academia and industry [2]. In recent years, benefiting from the rational design and innovation of non-fullerene molecules, the power conversion efficiencies (PCEs) of OSCs are constantly being refreshed and have exceeded 20 % thus far [3]. To achieve the commercial viability of OSCs, the high PCEs and long-term stability should be satisfied at the same time. However, the long-term stability of OSCs that

utilize small-molecule acceptors (SMAs) still faces challenges [4]. Among them, the degradation of optimal blended morphology may be the main factor for its poor stability when prolonged exposure to light or heat [5]. This is largely determined by the low glass transition temperature (T_g) and high diffusion coefficient of small molecules [6]. In response to these stability challenges, researchers have proposed the polymerized small-molecule acceptors (PSMAs) with multiple SMA units linked by benzodithiophene or thiophene etc [6a,7]. PSMAs have displayed the higher T_g and lower diffusion coefficient, thus making them more advantageous in stability compared to SMA. However, the disordered intermolecular stacking and lower crystallinity of PSMAs have resulted in a lower PCE of all-polymer OSCs [3e,8], compared to that of OSCs based on SMAs. Furthermore, all-polymer OSCs are still confronted with the challenge of batch-to-batch variations which is not conducive

* Corresponding authors.

E-mail addresses: zyao@nankai.edu.cn (Z. Yao), yschen99@nankai.edu.cn (Y. Chen).

¹ These authors contributed equally.

to large-scale preparation.

To overcome the above challenges, the emergence of oligomeric SMAs (OSMAs) that consist of a precise number of SMA units, is inspiring. These OSMAs maintained the potential in achieving excellent long-term stability because of the much higher T_g compared to SMAs [9]. Moreover, they also possess the well-defined molecular structures and good repeatability compared to PSMA. Consequently, OSMA could combine the advantages of SMA and PSMA successfully, and showed the great potential for preparing OSCs with excellent PCE and long-term stability simultaneously [6c,10]. The oligomeric SMAs (dimer and

multimer acceptors) were first explored in PDI based cores [11]. In 2013, Zhang designed a dimeric acceptor which linked two PDI groups by using a thiophene [11b]. Compared to monomeric PDI (0.13 %), the dimeric PDI possesses a much higher PCE of 4.03 %. Thereafter, by adapting this or similar design concept, a lot of exploratory work on OSMAs have been carried out [12]. However, compared to SMAs, OSMAs still lag behind in efficiency, mainly attributed to the relatively inferior fill-factor (FF) and short-circuit current density (J_{SC}) [13]. The root cause of this PCE gap may be caused by the reduction in molecular symmetry and planarity, which could decrease the intermolecular

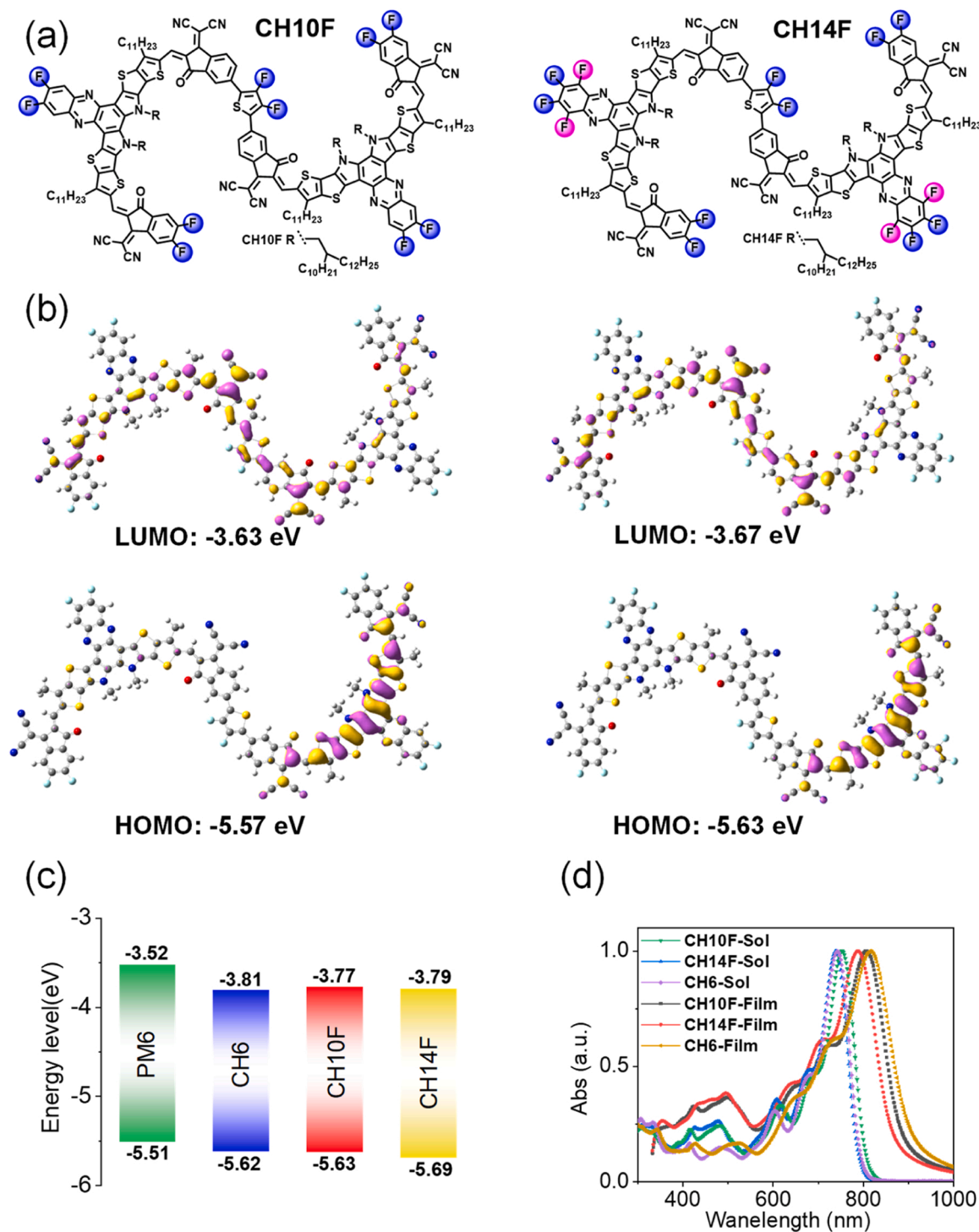


Fig. 1. (a) Chemical structures of CH10F and CH14F. (b) Spatial distributions of molecular frontier orbitals. The values of HOMO and LUMO energy levels were listed for a better comparison. (c) Energy levels derived from CV measurements. (d) UV-vis spectra in both solutions and solid films.

stacking strength and ordering.

Inserting enough heteroatoms, such as halogen atoms, into the peripheral active sites of molecules have been proven as an effective way to enhance the intermolecular packing force and form an ordered arrangement of molecules [14]. Among all the heteroatom candidates, fluorine is featured with the smallest atomic radius but largest electronegativity. Therefore, it plays an important role in regulating the intermolecular packing modes of acceptors and the nanoscale morphology of blend films [15]. Additionally, sufficient peripheral fluorination is also beneficial for obtaining the smaller exciton binding energies (E_b) of acceptors and achieving the efficient exciton dissociation even under a quite small driving force [16]. Currently, peripheral fluorination primarily occurs at the terminal unit of acceptors [17]. However, when introducing too many fluorine atoms to terminal units, the lowest unoccupied molecular orbital (LUMO) energy levels of acceptors will drop greatly, leading to the mismatch with donors and decreasing open-circuit voltages of OSCs. Note that the CH-series acceptors developed by our group possess sufficient peripheral reactive sites on central units in addition to terminal units [14,18], which allows for the feasible fluorination not only at terminals but also at central units. Interestingly, the LUMO energy level of acceptors only experiences a slight downward shift if conducting sufficient or even complete fluorination on central units.

Bearing these in mind, on a two-dimensional (2D) conjugated extended molecular platform, the sufficient fluorine atoms were introduced into the dimeric molecular backbone, including central units, terminal units and connecting units (Fig. 1a). This provides a dimeric acceptor of CH14F with 14 fluorine atoms around the molecular skeleton, affording the most fluorine-rich molecular backbone among all the OSMAAs currently. Benefitting from the secondary interactions induced by fluorine atoms, CH14F achieved the tighter and more ordered molecular packing. This thus helps to establish a better charge carrier transport pathway in films comparing to the control of CH10F with 10 peripheral fluorine atoms only. By employing PM6 as a donor, PM6:CH14F binary devices achieved a good PCE of 18.36 %, with an excellent FF of 79.30 %. In contrast, PM6:CH10F only afforded a PCE of 16.38 % with a much lower FF of 74.45 %. In order to improve photovoltaic performance, CH6 was further added into PM6:CH14F blends to expand their absorption range. As a result, PM6:CH14F:CH6 ternary devices achieved an improved PCE of 19.72 % with an exciting FF of 80.25 %. More importantly, the PM6:CH14F device retained over 80 % of initial PCE after being continuously heated at 65 °C for 1032 h, providing a new insight into OSCs with excellent efficiency and stability simultaneously.

2. Results and discussions

The chemical structures of CH10F and CH14F were illustrated in Fig. 1a. The detailed description of molecular synthesis (Scheme S1 and S2) and characterized data/spectra have been summarized in Supporting Information. Notably, both the dimeric acceptors could achieve the satisfactory yields. The impact of more peripheral fluorination on the frontier molecular orbitals of acceptors was revealed by density functional theory (DFT) calculations. As shown in Figure S1, both CH10F and CH14F exhibit relatively planar geometric shapes, but there is a significant difference in their dipole moments (0.97 Debye for CH10F and 1.70 Debye for CH14F). If the similar molecular skeletons were applied, a larger dipole moment may promote the more compact and ordered packing of molecules, consequently, enlarge the FFs of OSCs through improving charge transport dynamic in blend films [19]. The highest occupied molecular orbitals (HOMOs) and LUMOs of CH10F and CH14F were illustrated in Fig. 1b. The HOMOs and LUMOs are alternately distributed across the central donor and terminal acceptor segments of molecular backbones, respectively, indicating an effective intramolecular charge transfer (ICT) [20]. Compared to CH10F, the HOMO energy level of CH14F is lowered by 0.06 eV, while the LUMO energy

level is only lowered by 0.04 eV. Comparing to the fluorination at terminals, peripheral fluorination at the central unit could not only increase the fluorine density significantly but also minimize the downward shift of LUMO energy levels, thus preserving the high open-circuit voltage advantage. This manifests the advantages of central fluorination over terminal fluorination as we discussed above, especially for the delicately control of LUMOs. As shown in Figure S2, electrostatic potential (ESP) maps reveal that the central framework of CH10F exhibits a significantly higher electron-rich character compared to CH14F, which is consistent with the downshifted HOMO energy level of CH14F.

Cyclic voltammetry (CV) characterization of films determines the HOMO/LUMO energy levels to be - 5.63 eV/ - 3.77 eV for CH10F and - 5.69 eV/ - 3.79 eV for CH14F (Fig. 1c and Figure S3). The reversal tendency of LUMO energy levels alignment from single molecules (DFT calculation) to solid films (CV) suggests the different molecular packing behaviors of CH10F and CH14F. The energy gap of CH10F is 1.86 eV, whereas that of CH14F is 1.90 eV. Furthermore, to assess the light-harvesting capabilities of CH10F and CH14F, their absorption spectra in both solutions and solid films were recorded and depicted in Fig. 1d. In diluted solutions, the maximum absorption peaks of CH10F and CH14F appeared at 753 and 739 nm, respectively (Table S1). The corresponding optical bandgaps of CH10F and CH14F were evaluated to be 1.45 and 1.48 eV, respectively, by comparing their absorption edges of neat films. Compared to CH10F, the absorption spectra of CH14F in both solution and film exhibit an obvious blue shifting, which could be primarily attributed to the more peripheral fluorination and agrees well with the CV results (Fig. 1c). Notably, the enlarged molar extinction coefficients for CH14F could be observed in solutions ($2.47 \times 10^5 \text{ M}^{-1} \text{ cm}^{-1}$), comparing to that of CH10F with $1.76 \times 10^5 \text{ M}^{-1} \text{ cm}^{-1}$ (Figure S4), underscoring the enhanced light absorption conferred by the complete peripheral fluorination. To investigate the effect of peripheral fluorination on electron transport, we measured the electron mobility of CH10F and CH14F pure films by the space charge limited current (SCLC) measurements (Figure S5). CH14F demonstrated a larger electron mobility of $5.19 \times 10^{-4} \text{ cm}^2 \text{ V}^{-1} \text{ s}^{-1}$ than that of $3.69 \times 10^{-4} \text{ cm}^2 \text{ V}^{-1} \text{ s}^{-1}$ for CH10F, which is consistent with our hypothesis that additional fluorination improves acceptor-mediated charge transport.

As we have mentioned above, sufficient peripheral fluorination is expected to induce the more compact and orderly stacking of molecules, thereby improving FFs of OSCs. Thus, we utilized grazing-incidence wide-angle X-ray scattering (GIWAXS) to elucidate the potentially positive impact of more peripheral fluorination (Fig. 2a and 2b) [21]. As depicted in the line-cut profiles from Fig. 2c, 2d and the parameters summarized in Table S2, both CH10F and CH14F exhibit the strong (010) peaks in the out-of-plane (OOP) direction, indicative of a face-on stacking arrangement. Notably, the intermolecular π - π stacking distance ($d_{\pi-\pi}$) and crystal coherence lengths (CCLs) of (010) peaks along the OOP direction were measured to be 3.79 and 26.06 Å for CH14F, while 3.81 and 25.36 Å for CH10F, respectively. Additionally, the d-spacings/CCLs of the (100) peaks along the in-plane (IP) direction were 20.87/61.47 Å for CH10F and 20.60/68.96 Å for CH14F (Table S2). Apparently, the intermolecular packing distances slightly decrease but the CCLs increase in both OOP and IP directions after more peripheral fluorination on central units, suggesting a tighter and ordered molecular arrangement in CH14F film.

When molecules are arranged in a tight and organized stack, it may promote the delocalization of exciton vibrational relaxation across several molecules, which is beneficial for more efficient exciton dissociation. Therefore, we conducted the temperature-dependent photoluminescence (PL) measurements to evaluate the energy barrier (E_b) for charge separation (similar to exciton binding energy) of CH10F and CH14F in their neat films [14]. As illustrated in Fig. 2e, 2f and S6, the variation of PL intensity along with the temperature could reflect the recombination of charge carriers back into emitting excitons [22]. Therefore, the quite small E_b of ~ 35 meV for CH10F and ~ 30 meV for CH14F have been afforded (Figure S6). It is worth noting that the

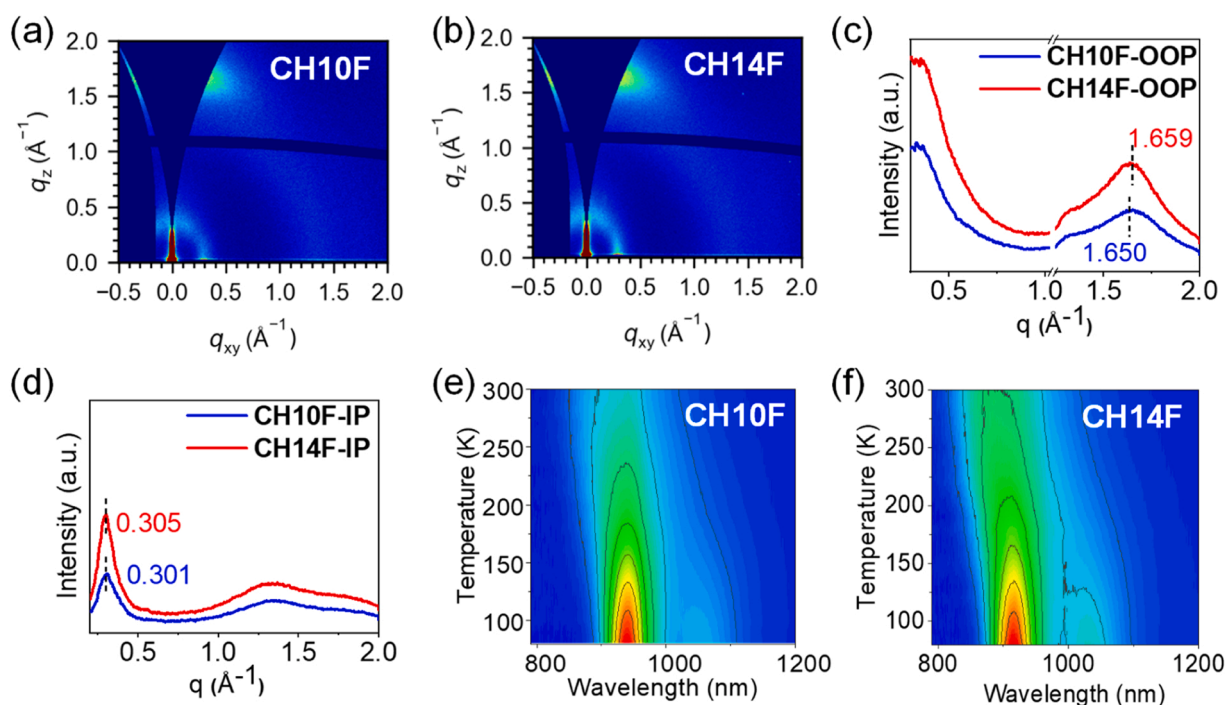


Fig. 2. (a, b) 2D GIWAXS patterns of neat films, respectively. (c, d) Line-cut profiles of CH10F and CH14F neat films. (e, f) The temperature-dependent PL spectra of neat film.

absolute values of E_b are hard to be obtained by temperature-varying PL herein, only the relative varying tendency between similar molecules is meaningful. This favorable characteristic of photogenerated excitons in CH14F films can boost effective exciton dissociation even driven by a quite small energy offset, meanwhile, suppress the non-radiative recombination from charge transfer (CT) states [23]. Furthermore, the pristine film of CH14F exhibits a higher dielectric constant (ϵ_r) of 3.74 than 3.56 for CH10F (Figure S7), which aligns with its larger dipole moment and stronger intermolecular interactions. The enhanced ϵ_r may facilitate charge generation/migration, thereby contributing to improved FF and J_{SC} .

In light of the proven advantages of more peripheral fluorination, the high-performance OSCs based on CH14F is expected. Herein, photovoltaic devices with a ITO/PEDOT:PSS/D:A blends/PNDIT-F3N/Ag architecture were fabricated (Fig. 3a). Upon blending with the well-matched polymer donor of PM6 (Figure S8), OSCs based on PM6:CH10F achieved a PCE of 16.38 % (Table 1), along with a V_{OC} of 0.919 V, a J_{SC} of 24.03 mA cm⁻², and an FF of 74.45 %. In contrast, after more peripheral fluorination on CH14F backbone, the PM6:CH14F-based OSCs exhibited a larger V_{OC} (0.930 V) and J_{SC} (25.04 mA cm⁻²), yet demonstrated a significantly enlarged FF of 79.30 %. Apparently, the more compact and ordered molecular stacking of CH14F should response for these improvements. What is more exciting is that when CH6 is introduced into the binary devices based on PM6:CH14F, the resulting ternary device reaches an excellent PCE of 19.72 %, primarily due to the further enhancement of a J_{SC} (27.93 mA cm⁻²) and FF (80.25 %) (Table 1 and Figure S9). The device fabrication details and photovoltaic data were presented in Supporting Information (Table S3–S20), and the best current density-voltage ($J-V$) curves of PM6:CH10F-, PM6:CH14F- and PM6:CH14F:CH6-based OSCs were shown in Fig. 3b. The external quantum efficiencies (EQEs) of three OSCs were also measured and illustrated in Fig. 3c. The integrated J_{SC} can be calculated as 23.06, 23.85 and 26.57 mA cm⁻² for PM6:CH10F, PM6:CH14F and PM6:CH14F:CH6-based OSCs, respectively, matching well with their $J-V$ tests. In comparison with the binary devices of PM6:CH14F, one of the reasons for the enhanced J_{SC} in ternary devices of PM6:CH14F:CH6 is the expansion of photoelectric response from

900 nm to nearly 950 nm which is attributed to CH6's broad absorption (Fig. 1d). Concurrently, a significant increase, even surpassing 90 % at 500–600 nm (Fig. 3c) in the EQE intensity for the PM6:CH14F:CH6 has been observed. This should be caused by some tangled factors, for example, the improved charge generation/transport, light harvesting or suppressed charge recombination, etc.

To disclose the root cause of better J_{SC} s and FFs for PM6:CH14F and PM6:CH14F:CH6-based OSCs, a systematic study has been performed. Firstly, the exciton dissociation efficiency (P_{diss}) was approximately evaluated by measuring the photoluminescence (PL) quenching of the blend films (Figure S10). CH14F possessed the higher P_{diss} of 95.69 %, compared to CH10F with 91.60 %. And then we measured the dependence of the photocurrent density (J_{ph}) on the effective voltage (V_{eff}) as shown in Fig. 3d. The exciton dissociation probability (η_{diss})/charge collection efficiency (η_{coll}) values for the PM6:CH10F, PM6:CH14F and PM6:CH14F:CH6-based devices were found to be 95%/80 %, 98%/90 %, and 98%/92 %, respectively (Fig. 3d). The larger η_{diss}/η_{coll} values for CH14F-based devices suggest the more efficient charge generation and exciton dissociation, agreeing with their larger EQEs. Furthermore, transient photocurrent (TPC) decay analysis (Figure S11) reveals a shorter charge extraction time for the CH14F-based device (0.25 μ s) compared to that of 0.38 μ s for CH10F. Concurrently, transient photovoltage (TPV) decay fitting (Figure S11) demonstrates a longer charge carrier lifetime in the PM6:CH14F binary device (186 μ s) than PM6:CH10F (121 μ s). Those results disclose the superior charge extraction and suppressed charge recombination in CH14F system. Based on the SCLC measurements (Fig. 3e), the electron (μ_e) and hole mobilities (μ_h) of blend films could be roughly estimated, being 2.83×10^{-4} and 3.39×10^{-4} cm² V⁻¹ s⁻¹ for PM6:CH14F and 3.24×10^{-4} and 3.53×10^{-4} cm² V⁻¹ s⁻¹ for PM6:CH14F:CH6. Both of them surpassed the 1.76×10^{-4} and 2.54×10^{-4} cm² V⁻¹ s⁻¹ for PM6:CH10F. Besides, the devices based on CH14F exhibit a more balanced μ_h/μ_e ratio of 1.20 and 1.09, comparing to that of 1.44 for CH10F. The higher and more balanced charge mobilities observed in the CH14F-based device should be attributed to the tight and orderly molecular stacking caused by more peripheral fluorination, thereby leading to the improved J_{SC} and FF.

Furthermore, the charge recombination behaviors were analyzed

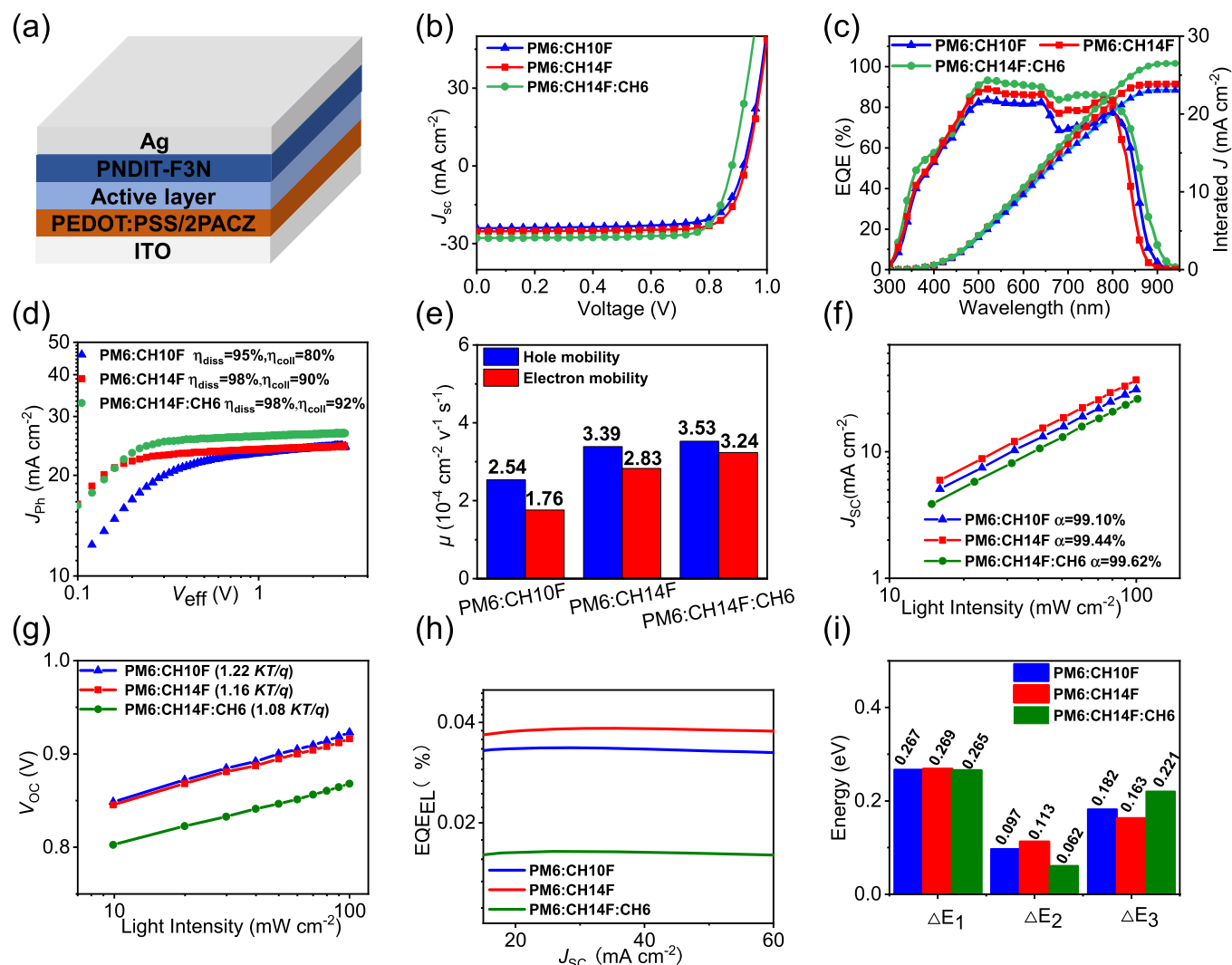


Fig. 3. (a) Schematic diagram of the device architectures. (b) J–V curves for OSCs. (c) EQE plots and integrated J_{SC} curves. (d) J_{ph} versus V_{eff} curves indicating η_{diss} and η_{col} . (e) Hole and electron mobilities of the OSCs. (f) Light intensity (P_{light}) dependence of J_{sc} . (g) Light intensity (P_{light}) dependence of V_{OC} . (h) The spectra of electroluminescence EQE. (i) E_{loss} and detailed three parts of ΔE_1 , ΔE_2 and ΔE_3 values of OSCs.

Table 1
Summary of device parameters of the optimized OSCs.

Active layers	V_{OC} (V)	J_{SC} (mA cm^{-2})	$J_{SC}^{cal,b}$ (mA cm^{-2})	FF (%)	PCE (%)
PM6:CH10F	0.919 (0.915 ± 0.007)	24.03 (23.96 ± 0.39)	23.06	74.45 (73.60 ± 3.08)	16.38 (16.04 ± 0.28)
PM6:CH14F	0.930 (0.927 ± 0.006)	25.04 (24.93 ± 0.29)	23.85	79.30 (78.95 ± 0.46)	18.36 (18.19 ± 0.17)
PM6:CH6	0.858 (0.859 ± 0.005)	27.56 (26.83 ± 0.73)	26.24	77.86 (79.19 ± 1.33)	18.33 (18.13 ± 0.20)
PM6:CH14F:CH6	0.881 (0.876 ± 0.003)	27.93 (27.83 ± 0.10)	26.57	80.25 (79.59 ± 1.27)	19.72 (19.29 ± 0.43)

^aAverage parameters derived from 10 independent OSCs (Table S15–S20).

^bCurrent densities calculated from EQE curves.

and shown in Fig. 3f and 3g. Firstly, the J_{SC} versus light intensity (P_{light}) dependency curves of all devices presented the slopes that are approaching unity, suggesting the greatly suppressed bimolecular recombination. Next, the dependence of V_{OC} on P_{light} rendered an $S/(kT/q)$

value of 1.22 for PM6:CH10F, 1.16 for PM6:CH14F and 1.08 for PM6:CH14F:CH6, suggesting the stepwise suppressed trap-assisted charge recombination[24]. The EQEs for electroluminescence (EQE_{EEL}) of PM6:CH10F, PM6:CH14F and PM6:CH14F:CH6 based devices were presented in Fig. 3h with the non-radiative energy losses estimated to be 0.182, 0.163 and 0.221 eV, respectively (Fig. 3i, S12 and Table S21) [23b]. The reduction in non-radiative energy losses for PM6:CH14F-based OSCs can be attributed to the improved molecular packing features and nanoscale film morphology, which also underscore the advantages of more peripheral fluorination on dimeric acceptors.

The improved device performances for OSCs are mainly owing to the more efficient charge generation/collection processes. These enhancements are closely associated to the optimized morphologies of active layers. Therefore, atomic force microscopy (AFM) was performed to reveal the surface morphologies of blend films and the quite uniform and smooth surfaces could be observed generally for all the blend films (Fig. 4a and S13). In particular, PM6:CH14F:CH6 displayed a smoother surface morphology, indicated by a slightly smaller root-mean-square roughness (R_q) value of 0.77 nm, compared to PM6:CH10F (0.84 nm) and PM6:CH14F blends (0.81 nm). AFM-based infrared spectroscopy (AFM-IR) was further employed to detect the D/A interpenetrating structures. Herein, we use the specific infrared (IR) absorption at 2215 cm^{-1} to detect the acceptors (Fig. 4b). By performing a

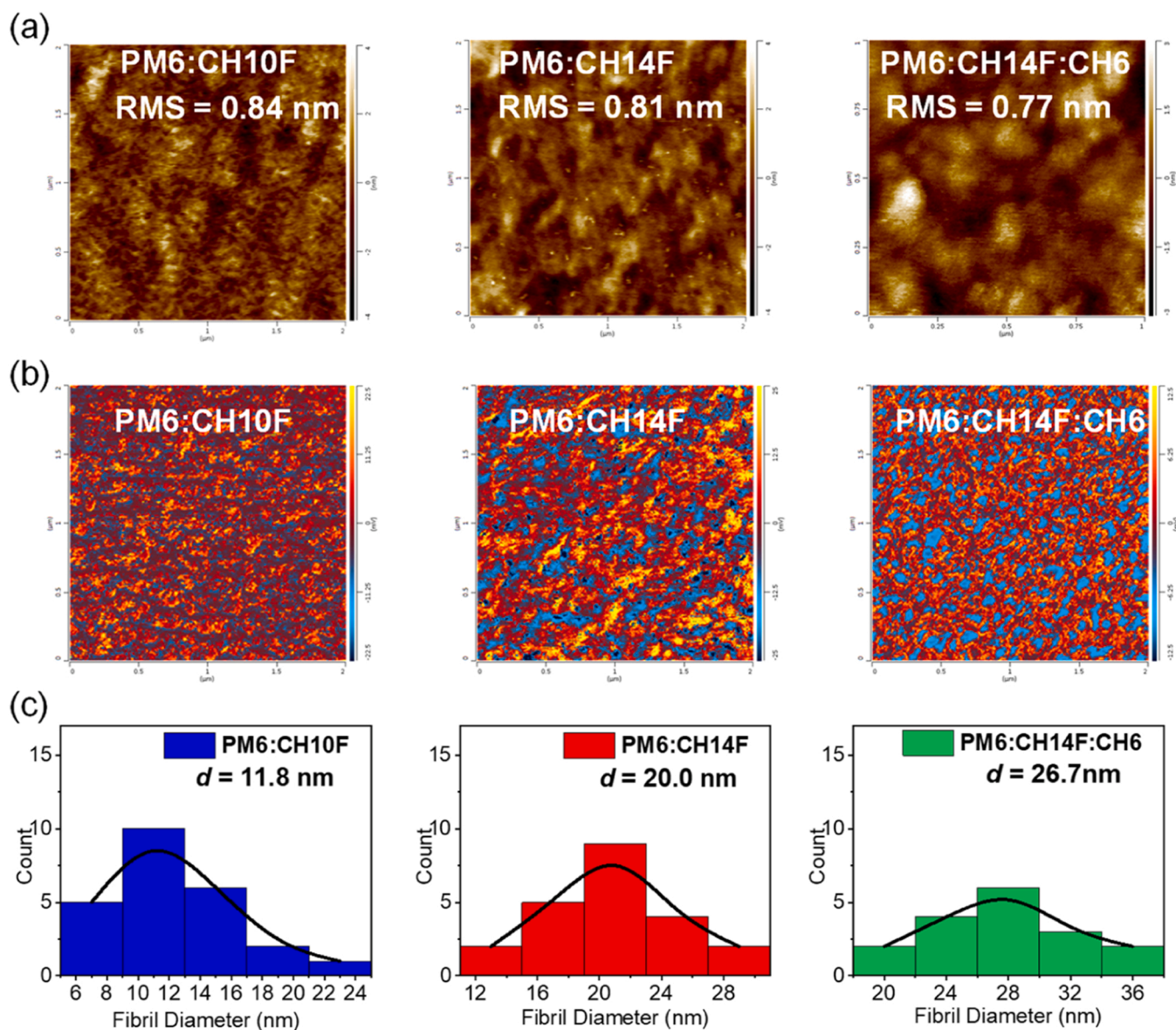


Fig. 4. (a) AFM height and (b) AFM-IR images recorded at 2215 cm^{-1} of the blend films. (c) Statistical distribution of fibril diameters for blend films.

statistical analysis of phase size (Fig. 4c), a gradually enlarged fibril diameter can be observed as 11.8, 20.0 and 26.7 nm for PM6:CH10F, PM6:CH14F and PM6:CH14F:CH6, respectively, suggesting the enhanced molecular crystallinity after more peripheral fluorination. Separation phase size correlates with the miscibility of PM6 and acceptors. Therefore, the surface tension (γ) and D/A miscibility were further assessed by measuring the contact angles (Figure S14 and Table S22). The compatibility of donor and acceptor was evaluated by calculating the Flory–Huggins interaction values (χ) [25]. Here, CH14F:CH6 has a χ value of 0.25, which is slightly higher than those of CH14F (0.17) and CH10F (0.13) (Figure S14 and Table S22). Such contributions might account for the enlarged separation phase size in PM6:CH14F:CH6 blends, which also aligns with the AFM-IR data (Fig. 4b).

The molecular packing behaviors in blend films were also unveiled by recording their GIWAXS patterns (Fig. 5a~5c and S15). All the blends afford the clear (010) peaks in the OOP direction and (100) diffraction in the IP direction, suggesting a dominant face-on molecular packing orientation (Fig. 5d, 5e and S15). In detail, the blend films exhibited a pronounced (010) diffraction peaks at 1.677 \AA^{-1} for PM6:CH10F, 1.686 \AA^{-1} and 1.702 \AA^{-1} for PM6:CH14F and PM6:CH14F:CH6 in OOP

directions (Fig. 5d and Table S2), the smaller π - π stacking distance of 3.73 \AA and 3.69 \AA for PM6:CH14F and PM6:CH14F:CH6 blends can be afforded comparing to that of 3.75 \AA for CH10F-based one (Fig. 5f). Furthermore, the slightly larger CCLs for PM6:CH14F (29.30 \AA) and PM6:CH14F:CH6 (32.13 \AA) can be also observed than that of 26.30 \AA for PM6:CH10F (Figure S16 and Table S2), indicating more ordered molecular packings in CH14F-based blends. PM6:CH14F and PM6:CH14F:CH6 possess shorter π - π stacking distance (21.59 \AA and 21.44 \AA) and larger CCLs (78.54 \AA and 84.40 \AA) compared to PM6:CH10F (21.89 \AA and 74.41 \AA) in IP direction (Fig. 5f, S16 and Table S2). Generally, the enhanced charge migration and higher FF observed in OSCs based on CH14F blends can be attributed to the more compact π - π stacking.

To investigate the effect of the peripheral fluorination on stability, thermal stability, storage stability and photostability of the devices based on CH10F and CH14F were evaluated (Figure S17, Figure S18 and Figure S19). The initial efficiency of the unencapsulated PM6:CH14F-based devices was 18.06 %, and still retained 80 % after 1032 h under continuous heating at $65\text{ }^\circ\text{C}$. On the contrary, devices based on PM6:CH10F rapidly degrade under the same conditions and have already decayed to 82 % of the initial PCE after 240 h (Figure S17). In addition,

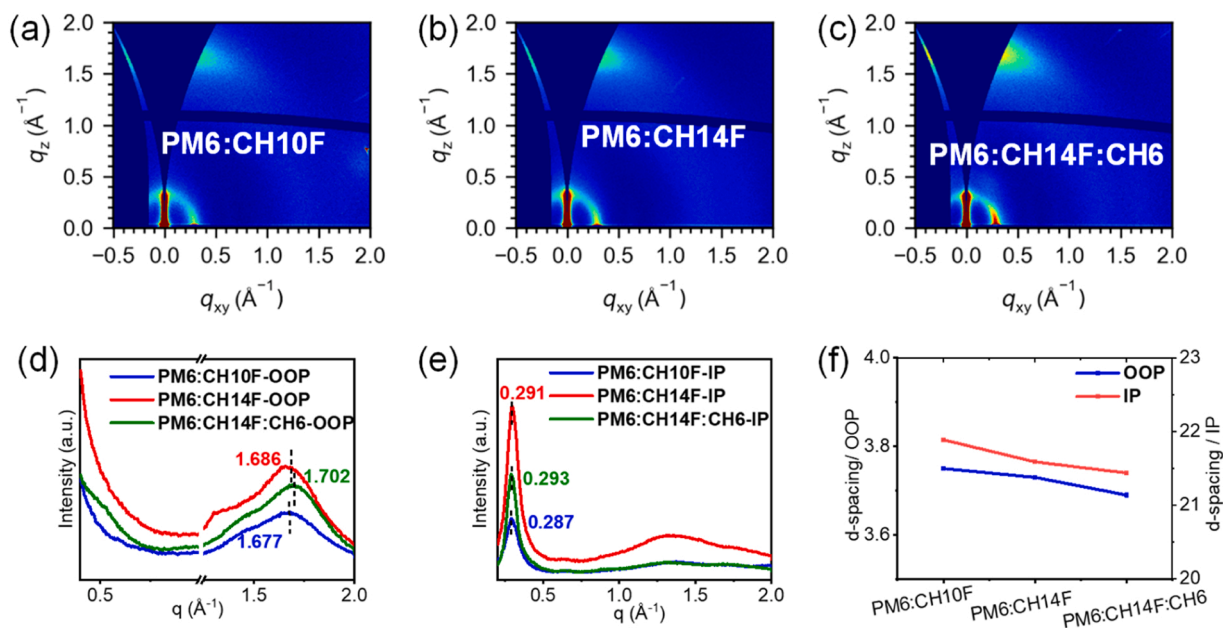


Fig. 5. (a–c) 2D GIWAXS patterns of the optimized blend films of OSCs. (d, e) Line-cut profiles of PM6:CH10F, PM6:CH14F and PM6:CH14F:CH6 blend films. (f) The d-spacing of (010) in OOP direction and (100) in IP direction for blend films.

for devices located in nitrogen glove box at the room temperature, approximately 89 % of their initial PCE could be maintained after 3792 h for devices based on CH14F (Figure S18), while only 84 % of their initial efficiency was maintained after 504 h for devices based on CH10F (Figure S18). Furthermore, the PM6:CH14F binary device maintained the 87.39 % of its initial performance after 185 h under 1 sun illumination, while the PM6:CH10F device showed the faster degradation, retaining only 81.14 % of its PCE over the equivalent time period (Figure S19). This sharply contrasting difference could be attributed to the more fluorine induced secondary interactions, which enhanced the morphology stability of blend films of CH14F (Figure S20).

3. Conclusion

In order to overcome the defects of oligomeric SMAs caused by the reduction in molecular symmetry and planarity, sufficient fluorine atoms were introduced into the active sites of molecular skeleton, providing a dimeric acceptor of CH14F containing 14 peripheral fluorine. Benefiting from the enhanced intermolecular secondary interactions induced by more fluorine, CH14F exhibits the stronger and more ordered molecular stacking comparing to its control molecule of CH10F with only 10 peripheral fluorine atoms. This favorable molecular stacking feature of CH14F helps to establish a better charge carrier transport pathway in blend films. Therefore, OSCs based on PM6:CH14F achieved a good PCE of 18.36 % with an excellent FF of 79.30 %, which is far superior to the OSCs based on CH10F with 16.38 % PCE and 74.45 % FF. By further employing CH6 as a third component, PM6:CH14F:CH6-based ternary OSCs afford an increased PCE of 19.72 % and more exciting FF of 80.25 %. More importantly, the device based on PM6:CH14F maintained over 80 % of its initial PCE after continuous heating at 65 °C for 1032 h, while the T_{80} of PM6:CH10F was only 240 h. By constructing such a 14 fluorine-containing or the most fluorine-rich OSMA, our work highlights the great importance of sufficient fluorination (especially central fluorination) in overcoming the inferior intermolecular stacking strength and ordering caused by the reduction in molecular symmetry and planarity, especially, provides a potential pathway to establish OSMA-based OSCs with excellent efficiency and stability simultaneously.

CRediT authorship contribution statement

Chen Yongsheng: Writing – review & editing, Writing – original draft, Project administration, Methodology, Investigation, Funding acquisition, Data curation, Conceptualization. **Ding Shuhui:** Methodology, Investigation. **Li Chenxi:** Methodology, Investigation, Data curation. **Wan Xiangjian:** Methodology, Investigation, Formal analysis, Data curation. **Long Guankui:** Software, Methodology, Investigation. **Guo Yaxiao:** Software, Methodology, Investigation. **Liang Huazhe:** Investigation. **Yao Zhaoyang:** Writing – review & editing, Writing – original draft, Methodology, Investigation, Data curation, Conceptualization. **Yang Jinyi:** Investigation. **Bi Xingqi:** Methodology, Investigation. **Cao Xiangjian:** Investigation.

Author contributions

S. D. and X. B. contributed equally to this work. The synthetic works were carried out by X. B.; the device optimizations and measurements were carried out by S. D.; J. Y. performed the DFT calculations; Y. C. and Z. Y. conceived and directed the study, wrote the manuscript. X. C., H. L., G. L., C. L., X. W. et al. helped to analyze the data and commented on the manuscript.

Declaration of Competing Interest

The authors declare that they have no known competing financial interests or personal relationships that could have appeared to influence the work reported in this paper.

Acknowledgements

The authors gratefully acknowledge the financial support from Ministry of Science and Technology of the People's Republic of China (National Key R&D Program of China, 2022YFB4200400), National Natural Science Foundation of China (52025033, 51873089, 22204119, 22309090, 22474089, 22479081), Natural Science Foundation of Tianjin (23JCZDJC00140) and Haihe Laboratory of Sustainable Chemical Transformations.

Appendix A. Supporting information

Supplementary data associated with this article can be found in the online version at [doi:10.1016/j.nanoen.2025.111008](https://doi.org/10.1016/j.nanoen.2025.111008).

Data availability

Data will be made available on request.

References

- [1] a) G. Zhang, J. Zhao, P.C.Y. Chow, K. Jiang, J. Zhang, Z. Zhu, J. Zhang, F. Huang, H. Yan, *Chem. Rev.* 118 (2018) 3447–3507;
b) T. Duan, Q. Chen, D. Hu, J. Lv, D. Yu, G. Li, S. Lu, *Trends Chem.* 4 (2022) 773–791;
c) C.B. Nielsen, S. Holliday, H.Y. Chen, S.J. Cryer, I. McCulloch, *Acc. Chem. Res.* 48 (2015) 2803–2812;
d) L. Dou, Y. Liu, Z. Hong, G. Li, Y. Yang, *Chem. Rev.* 115 (2015) 12633–12665.
- [2] Z. Wang, Y. Bo, P. Bai, S. Zhang, G. Li, X. Wan, Y. Liu, R. Ma, Y. Chen, *Science* 382 (2023) 1291–1296.
- [3] a) Z. Zheng, J. Wang, P. Bi, J. Ren, Y. Wang, Y. Yang, X. Liu, S. Zhang, J. Hou, *Joule* 6 (2022) 171–184;
b) L. Zhu, M. Zhang, J. Xu, C. Li, J. Yan, G. Zhou, W. Zhong, T. Hao, J. Song, X. Xue, Z. Zhou, R. Zeng, H. Zhu, C.-C. Chen, R.C.I. MacKenzie, Y. Zou, J. Nelson, Y. Zhang, Y. Sun, F. Liu, *Nat. Mater.* 21 (2022) 656–663;
c) T. Chen, S. Li, Y. Li, Z. Chen, H. Wu, Y. Lin, Y. Gao, M. Wang, G. Ding, J. Min, Z. Ma, H. Zhu, L. Zuo, H. Chen, *Adv. Mater.* 35 (2023) 2300400;
d) S. Wang, S. Wang, J. Wang, N. Yu, J. Qiao, X. Xie, C. Li, M.S. Abbasi, R. Ding, X. Zhang, Y. Han, G. Lu, J. Zhang, X. Hao, Z. Tang, Y. Cai, H. Huang, *Adv. Energy Mater.* (2025) 2405205;
e) C. Li, J. Song, H. Lai, H. Zhang, R. Zhou, J. Xu, H. Huang, L. Liu, J. Gao, Y. Li, M. H. Jee, Z. Zheng, S. Liu, J. Yan, X.-K. Chen, Z. Tang, C. Zhang, H.Y. Woo, F. He, F. Gao, H. Yan, Y. Sun, *Nat. Mater.* (2025), <https://doi.org/10.1038/s41563-024-02087-5>;
f) Y. Jiang, F. Liu, X. Zhu, *Nat. Energy* 9 (2024) 930–931;
g) X. Yu, P. Ding, D. Yang, P. Yan, H. Wang, S. Yang, J. Wu, Z. Wang, H. Sun, Z. Chen, L. Xie, Z. Ge, *Angew. Chem. Int. Ed.* 63 (2024) e202401518;
h) Y. Liu, B. Liu, C.-Q. Ma, F. Huang, G. Feng, H. Chen, J. Hou, L. Yan, Q. Wei, Q. Luo, Q. Bao, W. Ma, W. Liu, W. Li, X. Wan, X. Hu, Y. Han, Y. Li, Y. Zhou, Y. Zou, Y. Chen, Y. Liu, L. Meng, Y. Li, Y. Chen, Z. Tang, Z. Hu, Z.-G. Zhang, Z. Bo, *Sci. China Chem.* 65 (2022) 1457–1497;
i) R. Lin, Z. Luo, Y. Wang, J. Wu, T. Jia, W. Zhang, X. Gu, Y. Liu, L. Xiao, Y. Min, *Chem. Eng. J.* 503 (2025) 158635;
j) Y. Jiang, S. Sun, R. Xu, F. Liu, X. Miao, G. Ran, K. Liu, Y. Yi, W. Zhang, X. Zhu, *Nat. Energy* 9 (2024) 975–986;
k) L. Chen, J. Yi, R. Ma, T.A. Dela Pena, Y. Luo, Y. Wang, Y. Wu, Z. Zhang, H. Hu, M. Li, J. Wu, G. Zhang, H. Yan, G. Li, *Mater. Sci. Eng. R. Rep.* 159 (2024) 100794.
- [4] a) Y. Li, K.-K. Liu, F.R. Lin, A.K.Y. Jen, *Sol. Rrl* 7 (2023) 2300531;
b) P. Ding, D. Yang, S. Yang, Z. Ge, *Chem. Soc. Rev.* 53 (2024) 2350–2302387.
- [5] a) M. Ghasemi, H. Hu, Z. Peng, J.J. Rech, I. Angunawela, J.H. Carpenter, S. J. Stuard, A. Wadsworth, I. McCulloch, W. You, H. Ade, *Joule* 3 (2019) 1328–1348;
b) M. Ghasemi, N. Balar, Z. Peng, H. Hu, Y. Qin, T. Kim, J.J. Rech, M. Bidwell, W. Mask, I. McCulloch, W. You, A. Amassian, C. Risko, B.T. O'Connor, H. Ade, *Nat. Mater.* 20 (2021) 525–532;
c) N. Li, J.D. Perea, T. Kassari, M. Richter, T. Heumueller, G.J. Matt, Y. Hou, N. S. Gueldal, H. Chen, S. Chen, S. Langner, M. Berlinghof, T. Unruh, C.J. Brabec, *Nat. Commun.* 8 (2017) 14541;
d) M. Wu, B. Ma, S. Li, J. Han, W. Zhao, *Adv. Funct. Mater.* 33 (2023) 2305445.
- [6] a) Z.-G. Zhang, Y. Li, *Angew. Chem. Int. Ed.* 60 (2021) 4422–4433;
b) C. Zhang, J. Song, L. Ye, X. Li, M.H. Jee, H.Y. Woo, Y. Sun, *Angew. Chem. Int. Ed.* 63 (2024) e202316295;
c) J.-W. Lee, C. Sun, T.N.-L. Phan, D.C. Lee, Z. Tan, H. Jeon, S. Cho, S.-K. Kwon, Y.-H. Kim, B.J. Kim, *Energy Environ. Sci.* 16 (2023) 3339–3349.
- [7] a) Z. Luo, T. Liu, R. Ma, Y. Xiao, L. Zhan, G. Zhang, H. Sun, F. Ni, G. Chai, J. Wang, C. Zhong, Y. Zou, X. Guo, X. Lu, H. Chen, H. Yan, C. Yang, *Adv. Mater.* 32 (2020) 2005942;
b) J.-W. Lee, C. Sun, S.-W. Lee, G.-U. Kim, S. Li, C. Wang, T.-S. Kim, Y.-H. Kim, B. J. Kim, *Energy Environ. Sci.* 15 (2022) 4672–4685;
c) B. Liu, H. Sun, J.-W. Lee, J. Yang, J. Wang, Y. Li, B. Li, M. Xu, Q. Liao, W. Zhang, D. Han, L. Niu, H. Meng, B.J. Kim, X. Guo, *Energy Environ. Sci.* 14 (2021) 4499–4507;
d) G. Sun, X. Jiang, X. Li, L. Meng, J. Zhang, S. Qin, X. Kong, J. Li, J. Xin, W. Ma, Y. Li, *Nat. Commun.* 13 (2022) 5267;
e) H. Yu, Y. Wang, H.K. Kim, X. Wu, Y. Li, Z. Yao, M. Pan, X. Zou, J. Zhang, S. Chen, D. Zhao, F. Huang, X. Lu, Z. Zhu, H. Yan, *Adv. Mater.* 34 (2022) 2200361;
f) R. Sun, W. Wang, H. Yu, Z. Chen, X. Xia, H. Shen, J. Guo, M. Shi, Y. Zheng, Y. Wu, W. Yang, T. Wang, Q. Wu, Y. Yang, X. Lu, J. Xia, C.J. Brabec, H. Yan, Y. Li, J. Min, *Joule* 5 (2021) 1548–1565;
g) Z.-G. Zhang, Y. Yang, J. Yao, L. Xue, S. Chen, X. Li, W. Morrison, C. Yang, Y. Li, *Angew. Chem. Int. Ed.* 56 (2017) 13503–13507.
- [8] a) K. Nikaido, S. Inoue, S. Tsuzuki, R. Kumai, H. Matsui, K. Takaba, S. Maki-Yonekura, T. Yonekura, T. Hasegawa, *Phys. Rev. Mater.* 8 (2024) 115601;
b) L. Cao, H. Zhang, X. Du, X. Li, H. Lin, G. Yang, C. Zheng, S. Tao, *Chin. J. Chem.* 42 (2024) 3581–3587.
- [9] a) X. Gu, X. Zhang, H. Huang, *Angew. Chem. Int. Ed.* 62 (2023) e202308496;
b) Y. Liang, D. Zhang, Z. Wu, T. Jia, L. Luer, H. Tang, L. Hong, J. Zhang, K. Zhang, C.J. Brabec, N. Li, F. Huang, *Nat. Energy* 7 (2022) 1180–1190;
c) C. Sun, J.-W. Lee, C. Lee, D. Lee, S. Cho, S.-K. Kwon, B.J. Kim, Y.-H. Kim, *Joule* 7 (2023) 416–430;
d) H. Wang, C. Cao, H. Chen, H. Lai, C. Ke, Y. Zhu, H. Li, F. He, *Angew. Chem. Int. Ed.* 61 (2022) e202201844.
- [10] C. Sun, J.-W. Lee, Z. Tan, T.N.-L. Phan, D. Han, H.-G. Lee, S. Lee, S.-K. Kwon, B.J. Kim, Y.-H. Kim, *Adv. Energy Mater.* 13 (2023) 2301283.
- [11] a) Y. Lin, J. Wang, S. Dai, Y. Li, D. Zhu, X. Zhan, *Adv. Energy Mater.* 4 (2014) 1400420;
b) X. Zhang, Z. Lu, L. Ye, C. Zhan, J. Hou, S. Zhang, B. Jiang, Y. Zhao, J. Huang, S. Zhang, Y. Liu, Q. Shi, Y. Liu, J. Yu, *Adv. Mater.* 25 (2013) 5791–1405797;
c) D. Meng, D. Sun, C. Zhong, T. Liu, B. Fan, L. Huo, Y. Li, W. Jiang, H. Choi, T. Kim, J.Y. Kim, Y. Sun, Z. Wang, A.J. Heeger, *J. Am. Chem. Soc.* 138 (2016) 375–380.
- [12] a) F. Qi, Y. Li, R. Zhang, F.R.R. Lin, K. Liu, Q. Fan, A.K.Y. Jen, *Angew. Chem. Int. Ed.* 62 (2023) e202303066;
b) M. Lv, Q. Wang, J. Zhang, Y. Wang, Z.-G. Zhang, T. Wang, H. Zhang, K. Lu, Z. Wei, D. Deng, *Adv. Mater.* 36 (2024) 2310046;
c) Y. Li, J. Song, Y. Dong, H. Jin, J. Xin, S. Wang, Y. Ca, L. Jiang, W. Ma, Z. Tang, Y. Sun, *Adv. Mater.* 34 (2022) 2110155;
d) T. Wang, M. Chen, R. Sun, J. Min, *Chem* 9 (2023) 1702–2311767;
e) H. Qin, S. Ju, W. Su, B. Zhao, Q. Fan, Z. Bi, S. Zhang, J. Yu, G. Lu, J.-T. Hou, W. Ma, C. Gao, Y. Li, *J. Mater. Chem. C* 11 (2023) 750–758.
- [13] a) C. Wang, X. Ma, D. Deng, H. Zhang, R. Sun, J. Zhang, L. Zhang, M. Wu, J. Min, Z.-G. Zhang, Z. Wei, *Nat. Commun.* 15 (2024) 8494;
b) S.V. Dayneko, A.D. Hendsbee, G.C. Welch, *Small Methods* 2 (2018) 1800081.
- [14] Z. Yao, X. Cao, X. Bi, T. He, Y. Li, X. Jia, H. Liang, Y. Guo, G. Long, B. Kan, C. Li, X. Wan, Y. Chen, *Angew. Chem. Int. Ed.* 62 (2023) e202312630.
- [15] a) Y. Zou, H. Chen, X. Bi, X. Xu, H. Wang, M. Lin, Z. Ma, M. Zhang, C. Li, X. Wan, G. Long, Y. Zhaoyang, Y. Chen, *Energy Environ. Sci.* 15 (2022) 3519–3533;
b) L. Meng, S. Wu, X. Wan, Z. Shen, M. Li, Y. Yang, J. Wang, G. Lu, Z. Ma, Z. Yao, C. Li, Y. Chen, *Chem. Mater.* 34 (2022) 3168–3177;
c) S. Li, Y. Sun, B. Zhou, Q. Fu, L. Meng, Y. Yang, J. Wang, Z. Yao, X. Wan, Y. Chen, *ACS Appl. Mater. Interfaces* 13 (2021) 40766–40777;
d) H. Chen, Z. Zhang, P. Wang, Y. Zhang, K. Ma, Y. Lin, T. Duan, T. He, Z. Ma, G. Long, C. Li, B. Kan, Z. Yao, X. Wan, Y. Chen, *Energy Environ. Sci.* 16 (2023) 1773–1782.
- [16] a) L. Zhu, J. Zhang, Y. Guo, C. Yang, Y. Yi, Z. Wei, *Angew. Chem. Int. Ed.* 60 (2021) 15348–15353;
b) A. Ashokan, T. Wang, M.K. Ravva, J.-L. Bredas, *J. Mater. Chem. C* 6 (2018) 13162–13170.
- [17] D. Mo, H. Chen, Y. Zhu, H.-H. Huang, P. Chao, F. He, *ACS Appl. Mater. Interfaces* 13 (2021) 6147–6155.
- [18] H. Chen, Y. Zou, H. Liang, T. He, X. Xu, Y. Zhang, Z. Ma, J. Wang, M. Zhang, Q. Li, C. Li, G. Long, X. Wan, Z. Yao, Y. Chen, *Sci. China Chem.* 65 (2022) 1362–1373.
- [19] S. Li, C. He, T. Chen, J. Zheng, R. Sun, J. Fang, Y. Chen, Y. Pan, K. Yan, C.-Z. Li, M. Shi, L. Zuo, C.-Q. Ma, J. Min, Y. Liu, H. Chen, *Energy Environ. Sci.* 16 (2023) 2262–2273.
- [20] Z. Jia, S. Qin, L. Meng, Q. Ma, I. Angunawela, J. Zhang, X. Li, Y. He, W. Lai, N. Li, H. Ade, C.J. Brabec, Y. Li, *Nat. Commun.* 12 (2021) 178.
- [21] P. Mueller-Buschbaum, *Adv. Mater.* 26 (2014) 7692–7709.
- [22] Z. Zhang, S. Yuan, T. Chen, J. Wang, Y.-Q.-Q. Yi, B. Zhao, M. Li, Z. Yao, C. Li, X. Wan, G. Long, B. Kan, Y. Chen, *Energy Environ. Sci.* 17 (2024) 5719–5729.
- [23] a) F.D. Eisner, M. Azzouzi, Z. Fei, X. Hou, T.D. Anthopoulos, T.J.S. Dennis, M. Heeney, J. Nelson, *J. Am. Chem. Soc.* 141 (2019) 6362–6374;
b) X.-K. Chen, D. Qian, Y. Wang, T. Kirchartz, W. Tress, H. Yao, J. Yuan, M. Huelsbeck, M. Zhang, Y. Zou, Y. Sun, Y. Li, J. Hou, O. Inganäs, V. Coropceanu, J.-L. Bredas, F. Gao, *Nat. Energy* 6 (2021) 799–806;
c) J. Benduhn, K. Tvingstedt, F. Piersimoni, S. Ullbrich, Y. Fan, M. Tropicano, K. A. McGarry, O. Zeika, M.K. Riede, C.J. Douglas, S. Barlow, S.R. Marder, D. Neher, D. Spoltore, K. Vandewal, *Nat. Energy* 2 (2017) 17053.
- [24] L.J.A. Koster, V.D. Mihailetschi, R. Ramaker, P.W.M. Blom, *Appl. Phys. Lett.* 86 (2005) 123509.
- [25] S. Nilsson, A. Bernasik, A. Budkowski, E. Moons, *Macromolecules* 40 (2007) 8291–8301.



Shuhui Ding is a Ph.D student under the supervision of Prof. Yongsheng Chen at the College of Chemistry, Nankai University. Her current research focuses on the design and synthesis of organic photovoltaic materials.



Zhaoyang Yao received his Ph.D. degree from Changchun Institute of Applied Chemistry (CIAC), Chinese Academy of Sciences in 2016. Currently, he is a full professor in Department of Chemistry, Nankai University. His main research activities focus on the development of organic functional materials for various optoelectronic applications.



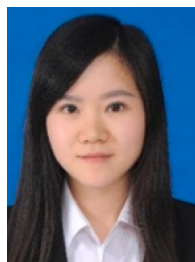
Xingqi Bi is a Ph.D student under the supervision of Prof. Yongsheng Chen at the College of Chemistry, Nankai University. His current research focuses on the design and synthesis of organic photovoltaic materials.



Guankui Long, a National Young Talent Scholar and Research Professor at Nankai University, earned his B.S. from Lanzhou University (2009) and Ph.D. from Nankai University under Prof. Yongsheng Chen. He conducted postdoctoral research at Tianjin Collaborative Innovation Center (Profs. Guan/Chen), University of Toronto (Prof. Sargent), and NTU (Profs. Gao/Soci). Since 2020, he leads an independent research group at Nankai focusing on chemistry and materials science.



Xiangjian Cao is a Ph.D student under the supervision of Prof. Yongsheng Chen at the College of Chemistry, Nankai University. His current research focuses on the design and synthesis of organic photovoltaic materials.



Yaxiao Guo received her Ph.D. degree from Changchun Institute of Applied Chemistry (CIAC), Chinese Academy of Sciences in 2018. Currently, she is a professor in Department of Chemistry, Tiangong University. Her main research involves the preparation of multifunctional nano and molecular catalysts, photocatalytic energy conversion, and novel solar cell devices.



Jinyi Yang is a Ph.D student under the supervision of Prof. Yongsheng Chen at the College of Chemistry, Nankai University. His current research focuses on the design and synthesis of organic photovoltaic materials.



Chenxi Li received his Ph.D. degree in Organic Chemistry from Nankai University, China, in 1990. Currently, he is a professor of Chemistry, Nankai University. His research interests focus on organic functional material design and synthesis.



Huazhe Liang received her Ph.D. degree from Nankai University in 2024 under the supervision of Prof. Yongsheng Chen. Her research focuses on the design and synthesis of organic photovoltaic materials.



Xiangjian Wan received his Ph.D. degree in Organic Chemistry from Nankai University, China, in 2006. Currently, he is a professor of Chemistry, Nankai University. His research interests focus on organic functional material design and application, especially on OPV material design and device optimization.



Yongsheng Chen received his Ph.D. in chemistry from the University of Victoria in 1997. From 2003, he has been a Chair Professor at Nankai University. His main research interests focus on carbon-based nanomaterials and organic functional materials for green energy application.